

Fault tolerant dynamical decoders for topological quantum memories

Michael Herold,^{1,*} Michael J. Kastoryano,² Earl T. Campbell,³ and Jens Eisert¹

¹*Dahlem Center for Complex Quantum Systems, Freie Universität Berlin, 14195 Berlin, Germany*

²*NBIA, Niels Bohr Institute, University of Copenhagen, 2100 Copenhagen, DK.*

³*Department of Physics and Astronomy, University of Sheffield, Sheffield S3 7RH, UK*

Active error correction of topological quantum codes – in particular the toric code – remains one of the most viable routes to large scale quantum information processing. In this work, we introduce the concept of a dynamical decoder as a promising route for achieving fault-tolerant quantum memories. We analyze a specific dynamical decoder based on a discrete time cellular automaton decoder and provide evidence of a threshold above 0.05 % with measurement errors. Without measurement errors, the threshold increases by a factor of roughly 1.5. We stress that (asynchronous) dynamical decoding gives rise to a Markovian dissipative process, hence equating cellular automaton decoding to a fully dissipative topological quantum memory, which removes errors continuously. Finally, we analyze the required resources, and speculate about an ideal constant resource dynamical decoder.

Quantum coherence is capricious, and taming it requires sophisticated methods of control and significant resource overhead. So far the best candidates are based on Kitaev's toric code [1, 2], and variants thereof. While quantum information can be stored in ground states of a toric Hamiltonian, thermal excitations are unconfined in two or three dimensions, allowing thermal diffusion and corrupting data in constant time [3, 4]. Using active decoding, this problem can be overcome. Errors must be regularly monitored by collecting syndrome information, which is analyzed by a decoding algorithm and corrected for. The first steps towards experimental implementations of error-correcting protocols are under way [5–8].

Given reliable snapshots of error syndromes, decoding algorithms can be independently applied to each time slice [9]. Decoders exist using notions of minimum-weight perfect matching [10], renormalisation [11, 12], and simulated annealing [13]. These techniques presuppose a global sharing of syndrome information, but more parallelized decoding is also possible with cellular-automaton decoders that locally store syndrome information, communicating with only nearest neighbors. Each node in the cellular-automaton stores a limited amount of additional data, and our focus here is on so-called ϕ -automata [14] where this data is a single variable, or ϕ -value, per node.

Yet, perfect syndrome measurement is a fantasy. It suffices for developing toy decoders, but is merely the first step to practical decoding. Conventionally, one tackles measurement errors by recording an entire history of syndrome snapshots, then running a decoder suitable for three-dimensional syndrome distributions. In contrast, here we propose the concept of a dynamical decoder, challenging the assumption that all errors must be corrected for in each time step; instead, they follow dynamical rules that gradually correct errors over time. Specifically, we show a ϕ -automaton decoder can tolerate measurement noise without significant changes to the algorithms, while preserving a number of desirable features. Measurement errors cause ripples in the dynamics, but may be naturally tolerated, provided fresh syndrome information is acquired before

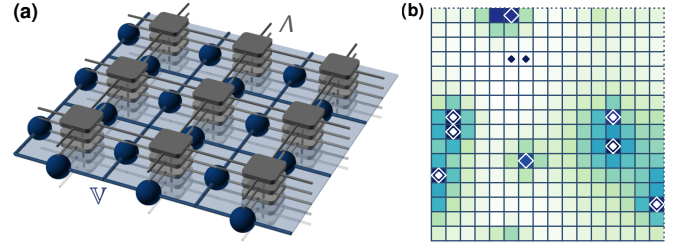


FIG. 1. (a) Layout of the decoder. Spheres represent toric code qubits and gray cells are interconnected elements of the cellular automaton, extending into the third dimension. (b) Snapshot of the asynchronous decoder on the toric code plane for a given numerical run. Filled diamonds represent actual anyons, empty diamonds correspond to measured -1 syndromes that act as field sources. The color scale represents the field intensity which builds up around anyons.

the ripple travels too far. No explicit record of the syndrome history is required, rather past syndromes merely leave echoes in the state of the cellular-automaton.

Apart from constituting a fresh way of devising fault-tolerant architectures, this dynamical paradigm has further applications to various physical implementations where syndromes can not easily be measured synchronously. In systems where entanglement is generated probabilistically [15–18], including syndrome measurements [19], this situation readily applies. Rather than a well defined series of snapshots, the syndromes are refreshed asynchronously; meaning that every unit cell of the cellular automaton decoder is updated with a certain probability that is independent of the other cells. We present here numerical evidence of a fault-tolerant threshold for quantum error correction by an asynchronous dynamical decoder. The dynamical paradigm is equally plausible in other architectures with an inherently modular structure of interacting nodes, as is notably the case in anticipated mesoscopic implementations of the toric code [20, 21], based on Majorana bound states supported by topological semi-conductor nanowires.

The locality and asynchronicity of such decoders makes them conceptually equivalent to certain physical systems undergoing open system dynamics. We show that an asynchronous cellular-automata decoder can be considered as the discretiza-

* m.herold@fu-berlin.de

tion of a Markovian master equation which dissipatively protects the topological subspace of the code. This opens up the potential of engineering quantum memories from locally interacting matter systems, providing passive protection against noise. In this sense, one can think of passive dissipative quantum memories protected against unwanted dissipation. Therefore, asynchronous dynamical decoders have potential applications across a broad spectrum of physical systems.

An asynchronous cellular-automaton is most naturally built from a synchronous cellular-automaton that does not require a clock or time dependent rules. One such time homogeneous cellular-automaton is provided by the 3D ϕ -automaton of Ref. [14]. In contrast, the 2D* ϕ -automaton of Ref. [14] and an automaton studied by Harrington [22] both keep track of time, and so are less easily adapted to an asynchronous setting. For completeness, we later review synchronous operation of the Harrington decoder. We show that our dynamical 3D ϕ -automaton decoder provides such an asynchronous dynamical decoder. In contrast, a dynamical decoder studied by Harrington [22, 23] relies on an exact series of events, and so is less easily adapted to the asynchronous setting. For completeness, we later review synchronous operation of this decoder. Finally, we discuss the possibility of a strictly constant resource dissipative self-correcting memory.

ϕ -automaton decoders. Decoders in our context are processes that remove errors from a lattice configuration \mathbb{V} and bring the system's state back to the code space. For simplicity in this letter we focus on the toric code and only consider uncorrelated Pauli X errors, measured by *plaquette operators*. Since Pauli Z errors can be treated in the same way, this does not restrict generality. To restrict ourselves to algorithms that can be highly parallelized and are inherently local, we formulate all algorithms as *cellular automata (CA)*. For every measurable syndrome in the code we also place a cell for the automaton, constituting a parallel lattice Λ with one cite per plaquette. The cell has local access to the measured syndrome and can read information from the neighboring cells on the CA lattice Λ . If a -1 syndrome is measured, we will say that an *anyon* is present. The anyons can be moved locally by applying (or equivalently storing) local bit flip operations. The automaton possesses the same periodic boundary conditions as the code does. As we will see, it is sometimes convenient to allow the CA lattice Λ to extend in the third dimension (see Fig. 1).

We specifically focus on and generalize a scheme for CA decoding the 2D toric code, introduced in Ref. [14]. The underlying idea is to simulate an attractive interaction between anyons from local update rules. The attraction is mediated via a scalar field $\phi(\mathbf{x})$ on the discrete lattice $\mathbf{x} \in \Lambda$. Sites occupied by anyons act as sources for the field. A field value is stored at each cell of the automaton, and the field builds up according to a local discretized version of Poisson's equation. As it turns out, the field has to be generated via a CA which extends into the third dimension so as to guarantee that the field falls off as $1/r$ away from anyons. That way, nearby anyons are attracted to each other under the influence of the field, but do not feel the attraction of far away anyons very strongly. Generating such a field locally in two dimensions seems to be difficult, but it occurs naturally in 3D. We will briefly review the so-called

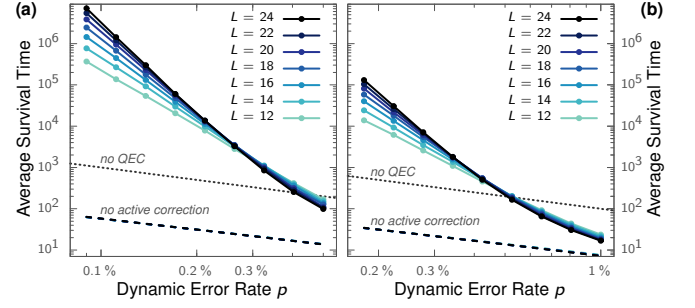


FIG. 2. Threshold in the average survival time of the dynamical 3D ϕ -automaton decoder with measurement errors ($q = p$) in (a) synchronous and (b) asynchronous operation. Asynchronous operation enables anyon movement with probability 1 instead of $1/2$. This increases the threshold by a factor 1.9. However, probabilistic measurements and field updates reduce the survival time at threshold compared to synchronous updates. The exact behavior depends on measurement and field update rates.

3D ϕ -automaton depicted in Fig. 1a.

The cellular automaton update rules dynamically evolve a combined quantum-classical system. For ease of presentation, the field and anyon positions are embedded in quantum systems with Hilbert spaces \mathcal{L} and \mathcal{V} , respectively. We use σ to denote states within the composite space $\mathcal{H} \otimes \mathcal{L} \otimes \mathcal{V}$, where \mathcal{H} is the toric code Hilbert space. The update rules are composed of two elementary components: field updates F and anyon updates A . The field update F simultaneously replaces the field value at all sites by the average of all six neighboring field values and adds $+1$ when an anyon is present. The anyon update A moves anyons to the one of their four neighboring sites in the toric code plane with the highest associated ϕ -value. Unwanted limit cycles are avoided by moving with a probability of $1/2$ only.

In order for two anyons to be attracted to each other, they must “feel” the field from the other anyon. In other words, the influence of an anyon on the field ϕ needs to have propagated to other anyons. To ensure a sufficient convergence of the field between anyon updates, it is required that F is applied $c \sim \log^2 L$ times. This yields the compound update rule $D_c := AF^c$. Applying the update D_c several times guarantees that typical clusters of errors get collapsed back to an anyon free configuration. When the error rate is below threshold, the system will be projected back to the original ground state with exponentially decreasing probability of error. See Ref. [14] for a detailed account of this ϕ -automaton, and for an analysis of its performance as a decoder.

Dynamical decoders. We next want to introduce the notion of a *dynamical decoder*, for the moment still in the synchronous setting. We denote by E_p the error map that applies X -flips on each qubit of the toric code with probability p . The incorrect error syndrome extraction is reflected by the application of a map M_q , where $q > 0$ denotes the probability that a syndrome is incorrect. For perfect syndrome measurement, $q = 0$, decoding can be achieved with only one round of syndrome extraction and a suitable number τ of updates D_c ,

$$\sigma_\tau = (D_c^\tau M_0 E_p)(\sigma), \quad (1)$$

where σ is a state on the combined quantum-classical Hilbert space. The exponent τ must be chosen such that the decoder terminates. If the error rate p is below a certain critical threshold, a logical error is returned with probability exponentially suppressed in L . However, for active error correction only *partial* decoding is necessary between different rounds of syndrome measurements. In particular, one may consider very short *sequences* in which only partial corrections are calculated before the syndrome is remeasured. We refer to this concept as *dynamical decoding*. Specifically, we define synchronous dynamical decoding as the succession of the maps

$$\sigma_\tau = (D_c M_q E_p)^\tau (\sigma), \quad (2)$$

where the integer τ is the number of sequences. In the setting of dynamical decoding, we are interested in estimating the survival time of the logical subspace; i.e. how long one typically has to wait before a logical X or Z error occurs on the encoded qubits. In order to determine this survival time we check whether a logical error has occurred by decoding a copy of the state without measurement errors in every sequence. Figure 2a presents the survival times for different system sizes as a function of the error rate obtained by simulating the dynamical decoding process with measurement errors $q = p$. Fitting a scaling law incorporating finite size effects indicates the existence of a threshold at $p = 0.16\%$. However, based on an in-depth analysis of field decoders incorporating system sizes up to $L = 80$ we expect a lower threshold within the range of 0.03 to 0.04% (see Appendix A).

Decoding in continuous time. Equation (2) defines synchronous dynamical decoding, where for the ϕ -automaton decoder the field updates F and the anyon updates A are applied simultaneously on all sites at each time step. A more physically relevant scheme would be one that is naturally *asynchronous*. We consider the local operators f_x and a_x performing field and anyon updates but only applied to a single site x , and the $X_{p,v}$ -operator applying a Pauli operator to the edge $v \in \mathbb{V}$ with probability p . The $m_{q,x}$ -operator reflects a measurement with error probability q at $x \in \Lambda$. We pick a site x (or edge v in the case of $X_{p,v}$) at random, and apply the local map to that site (or edge). The probability to choose f_x is weighted with $c \sim \log^2 L$. To compare the performance of synchronous and asynchronous dynamical decoders, we define one time step as the number of operations after which all anyons on average had the chance to move once. In Fig. 2b, the survival time of the asynchronous ϕ -automaton decoder is plotted as a function of system size and error rate, where we set $q = p$, suggesting a threshold at 0.3%. Further analysis determines a lower threshold between 0.05% to 0.08%.

Markovian dissipative decoding. An asynchronous cellular automaton can be understood as the evolution induced by a time independent Markovian master equation. At a constant rate, the coherent evolution is interrupted by quantum jumps corresponding to local unitary operations. Such a prescription precisely corresponds to a continuous one parameter semigroup, here acting on both the quantum state, as well as the effectively classical record of the anyon location and the classical auxiliary fields. The dynamical equation is given by $\partial\sigma/\partial t = \mathcal{L}(\sigma)$ where \mathcal{L} is the Liouvillian decom-

posed as $\mathcal{L} := \sum_j \mathcal{L}_j$ and each local term takes the form $\mathcal{L}_j(\sigma) = \gamma_j(L_j\sigma L_j^\dagger - L_j^\dagger L_j\sigma/2 - \sigma L_j^\dagger L_j/2)$. The $\{L_j\}$ are called Lindblad operators and $\{\gamma_j > 0\}$ can be viewed as the rates of the dissipative processes. Specifically, we construct a Liouvillian where the geometrically local jump operators L_j are constructed from $X_{p,v}$, $m_{q,x}$, f_x , and a_x , for all x and v , with corresponding weights $\{\gamma_X, \gamma_m, \gamma_f, \gamma_a\}$. The γ_f rates must now scale as $c \sim \log^2 L$ relative to all other rates to emulate the scaling of c in the previous paragraph. In other words, asynchronous dynamical decoding can be understood as a dissipative process

$$\mathcal{L} = \mathcal{L}_C + \mathcal{L}_E, \quad (3)$$

where the dissipative decoder reflected by \mathcal{L}_C continuously “corrects” an uncontrollable noise operator \mathcal{L}_E describing the actual noise. In this sense, the promise of “fighting noise with noise” is most manifestly realized. We hence naturally bridge the gap between decoding and dissipative self-correction [24, 25]. The Lindblad operators can be directly constructed from the local unitaries or stochastic maps of the update rules.

System size dependencies. The ϕ -automaton decoder is characterized by the simplicity of its update rules and is particularly amenable to a representation as an asynchronous CA. However, there are some mild system size dependencies hidden in the construction that need to be accounted for. The first obvious one is the necessity to run the field updates for a number of rounds of order $\text{polylog } L$ for every anyon move. Translated to the dissipative setting, this corresponds to the rates γ_f scaling as $\text{polylog } L$. In physical terms, this corresponds to the necessity of the field update operations to be increasingly fast with the size of the system. In practice, this is not much of an issue, as the field updates correspond to purely classical processing.

Secondly, in the rule for anyon displacement, we need the field to have a resolution that grows with the system size. If the field is encoded digitally, then this corresponds to a local dimension of the CA lattice that scales moderately as $\log \log L$. Finally, the anyon updates do not depend on the magnitude of the field, but rather move with unit probability, whenever there is a non-zero field gradient. This feature can also be adapted to the dissipative picture with a logarithmic overhead by digitally simulating a step function at the level of the jump operators. Thus, the CA decoder can naturally be represented as a local dissipative process, at the cost of merely logarithmically unbounded jump rates.

Dynamical decoders using directed signaling. A dynamical CA decoder analyzed by Harrington avoids the required logarithmic speedup of our 3D decoder [22, 26]. The basic working principle is analogous to traditional MWPM heuristics [27]. The subsequent fusion of anyons over larger and larger distances is realized via $\log_3 L$ hardware layers with each layer being responsible for a certain class of anyon distances. Most of the cells implement directed signaling between a few cells that coordinate the correction process. This approach requires inhomogeneous update rules, a certain structure inside the automaton and synchronous operation. The effective time scales are chosen such that the correction processes do not interfere between the layers. Reference [22] provides numerics suggesting a threshold between 0.01% and 0.1%. We benchmark a

simplified version of the original decoder with 2×2 colonies. We find that our data is consistent with a threshold below $p = 0.001\%$. The actual threshold is inaccessible due to finite size effects (see Appendix E).

Measurement errors. It is known that for many of the existing topological quantum codes, it is necessary to keep a log of the syndrome information whenever there are measurement errors. Only codes allowing for *single shot decoding* [28, 29] can cope with measurement errors in the setting of Eq. (1). One of the main benefits of both synchronous and asynchronous dynamical decoders is that measurement errors are naturally incorporated without any additional overhead. This feature is inherited from the local structure of the decoding algorithm: If the presence of an anyon is falsely indicated, this may only result in a single additional bit-flip error created by the local anyon move. In the next sequence this bit flip is likely incorporated into the syndrome and is not different from usual errors. Also, the imaginary anyon may attract other anyons, which is not different from the case where a real error occurred. Therefore, the presence of measurement errors simply corresponds to an effective shift of the error rate by a constant factor (see Appendix A).

Existence of constant overhead decoders. The fundamental challenge in building topological quantum memories is formulated in the established conjecture that, self-correcting quantum memories only exist in four or higher dimensions. This lead to the rule of thumb that 1D classical and 2D quantum memories share fundamental features and equally, 2D classical and 4D quantum memories. Classical memories in 2D can exhibit a thermal phase transition (e.g. 2D Ising model) and dynamical decoders with constant overhead exist (e.g. Toom’s rule). The same applies to the 4D toric code [2], where the idea of using dynamical decoding for dissipative self correction has already been studied [24]. While there are no thermal phase transitions in 1D for classical Hamiltonian systems, there do exist ordered phases in one dimensional interacting particle systems. This is constructively proven by the seminal work of Gács [30–32]. In the light of dynamical decoders, Gács’ cellular automaton can be interpreted as an asynchronous dynamical decoder that removes string-like excitations from classical 1D systems using only constant overhead. Harrington has speculated that

this ought to generalize to a two dimensional quantum code [22]. However, even in 1D, the Gács algorithm is tremendously complex with no numerical or experimental realization known to the authors. Analytic work estimates the Gács 1D threshold at $\sim 2^{-1000}$, so presently the outlook is poor for such an approach to yield a quantum decoder of practical relevance.

Discussion. In this work we introduced a novel type of decoders that are suited for operating on a large number of physical and logical qubits. Our proposal of a 3D ϕ -automaton as an asynchronous dynamical decoder shows that very simple algorithms with modest overhead can exhibit a threshold, even in the presence of measurement errors. Also, we have shown how new decoding algorithms provide a blueprint for engineering dissipative self-correction memories. The arguments given in Ref. [4] are likely to rule out the possibility to archive robustness in quantum memories by introducing additional terms in the Hamiltonian. Therefore, it seems imperative to circumvent no-go theorems for Hamiltonian self-correcting memories by either considering codes not covered by such theorems [33]; or to engineer dissipation that renders the code in effect self correcting. Our 3D ϕ -automaton decoder may not yet provide a final answer to those questions, since the corresponding Lindblad operators contain terms scaling as $\log^2 L$. In general the design of dynamical decoders seems to inherit a trade-off between the degree of complexity in the local rules and the scaling of the local resources. It provides a clear perspective, however, how such dissipative decoders can be designed.

The features of complete parallelization and asynchronous operation are not only relevant for the implementation also address the problem of wiring for on-chip architectures, (ex: Ref. [21]), and naturally incorporates asynchronous syndrome measurements, attractive for photonic chip based processors. Dynamical decoders are therefore particularly interesting playground for fault tolerance while providing intrinsic parallelization.

Acknowledgements. We thank Ben Brown and Barbara Terhal for helpful discussions and for carefully reading a draft. ETC is supported by the EPSRC (grant EP/M024261/1). MJK is supported by the Carlsbergfond and the Villum fond. JE is supported by the ERC (TAQ), the EU (RAQUEL, SIQS, AQuS), the DFG, and the BMBF (Q.com).

-
- [1] A. Y. Kitaev, in *Quantum communication, computing, and measurement* (Springer, 1997) pp. 181–188.
 - [2] E. Dennis, A. Kitaev, A. Landahl, and J. Preskill, *J. Math. Phys.* **43**, 4452 (2002).
 - [3] R. Alicki, M. Fannes, and M. Horodecki, *J. Phys. A* **42**, 065303 (2009).
 - [4] O. Landon-Cardinal, B. Yoshida, D. Poulin, and J. Preskill, *Phys. Rev. A* **91**, 032303 (2015).
 - [5] T. H. Taminiau, J. Cramer, T. van der Sar, V. V. Dobrovitski, and R. Hanson, *Nature Nano.* **9**, 171 (2014).
 - [6] G. Waldherr, Y. Wang, S. Zaiser, M. Jamali, T. Schulte-Herbruggen, H. Abe, T. Ohshima, J. Isoya, J. F. Du, P. Neumann, and J. Wrachtrup, *Nature* **506**, 204 (2014).
 - [7] L. Sun, A. Petrenko, Z. Leghtas, B. Vlastakis, G. Kirchmair, K. M. Sliwa, A. Narla, M. Hatridge, S. Shankar, J. Blumoff, L. Frunzio, M. Mirrahimi, M. H. Devoret, and R. J. Schoelkopf, *Nature* **511**, 444 (2014).
 - [8] J. Kelly, R. Barends, A. G. Fowler, A. Megrant, E. Jeffrey, T. C. White, D. Sank, J. Y. Mutus, B. Campbell, Y. Chen, Z. Chen, B. Chiaro, A. Dunsworth, I. C. Hoi, C. Neill, P. J. J. O’Malley, C. Quintana, P. Roushan, A. Vainsencher, J. Wenner, A. N. Cleland, and J. M. Martinis, *Nature* **519**, 66 (2015).
 - [9] B. Terhal, *Rev. Mod. Phys.* **87**, 307 (2015).
 - [10] A. G. Fowler, A. C. Whiteside, and L. C. L. Hollenberg, *Phys. Rev. A* **86**, 042313 (2012).
 - [11] G. Duclos-Cianci and D. Poulin, *Phys. Rev. Lett.* **104**, 050504 (2010).
 - [12] S. Bravyi and J. Haah, *Phys. Rev. Lett.* **111**, 200501 (2013).
 - [13] J. Wootton, “A simple decoder for topological codes,” (2013), [arXiv:1310.2393v3](https://arxiv.org/abs/1310.2393v3).

- [14] M. Herold, E. T. Campbell, J. Eisert, and M. J. Kastoryano, *Nature P. J. Quant. Inf.* **1** (2015), 10.1038/npjqi.2015.10.
- [15] C. Cabrillo, J. I. Cirac, P. Garcia-Fernandez, and P. Zoller, *Phys. Rev. A* **59**, 1025 (1999).
- [16] Y. L. Lim, A. Beige, and L. C. Kwek, *Phys. Rev. Lett.* **95**, 030505 (2005).
- [17] S. D. Barrett and P. Kok, *Phys. Rev. A* **71**, 060310 (2005).
- [18] E. T. Campbell and S. C. Benjamin, *Phys. Rev. Lett.* **101**, 130502 (2008).
- [19] N. H. Nickerson, Y. Li, and S. C. Benjamin, *Nature Comm.* **4**, 1756 (2013).
- [20] B. M. Terhal, F. Hassler, and D. P. DiVincenzo, *Phys. Rev. Lett.* **108**, 260504 (2012).
- [21] L. A. Landau, S. Plugge, E. Sela, A. Altland, S. M. Albrecht, and R. Egger, “Towards realistic implementations of a Majorana surface code,” [arXiv:1509.05345](https://arxiv.org/abs/1509.05345).
- [22] J. W. Harrington, *Analysis of quantum error-correcting codes: symplectic lattice codes and toric codes*, Ph.D. thesis (2004), http://thesis.library.caltech.edu/1747/1/jimh_thesis.pdf.
- [23] D. Michels, K. Duivenvoorden, and B. M. Terhal, “A local-finite speed decoder for the toric code,” (2015), in preparation.
- [24] F. Pastawski, L. Clemente, and J. I. Cirac, *Phys. Rev. A* **83**, 012304 (2011).
- [25] M. J. Kastoryano, M. M. Wolf, and J. Eisert, *Phys. Rev. Lett.* **110**, 110501 (2013).
- [26] K. Michnicki, *Towards self-correcting quantum memories*, Ph.D. thesis (2015).
- [27] D. Avis, *Networks* **13**, 475 (1983).
- [28] H. Bombin, “Single-shot fault-tolerant quantum error correction,” (2014), [arXiv:1404.5504v2](https://arxiv.org/abs/1404.5504v2).
- [29] B. J. Brown, N. H. Nickerson, and D. E. Browne, “Fault tolerance with the gauge color code,” [arXiv:1503.08217v1](https://arxiv.org/abs/1503.08217v1).
- [30] P. Gács, *J. Comp. Sys. Sc.* **32**, 15 (1986).
- [31] P. Gács, *J. Stat. Phys.* **103**, 45 (2001).
- [32] L. F. Gray, *J. Stat. Phys.* **103**, 1 (2001).
- [33] C. G. Brell, “A proposal for self-correcting stabilizer quantum memories in 3 dimensions (or slightly less),” (2014), [arXiv:1411.7046v2](https://arxiv.org/abs/1411.7046v2).

Appendix A: Detailed Numerical Analysis of Dynamical ϕ -Automaton Decoders

1. Estimation of Thresholds

The simulation of dynamical 3D ϕ -automaton decoders on traditional architecture is numerically expensive. The fact that the simulation has to run throughout the full survival time, which grows very rapidly with increasing system size and decreasing error rates. Furthermore, we simulate the 3D cellular automata within a serial centralized computing model, which leads to an additional time cost scaling with L^3 . Parallelisation exploiting the cellular nature of the decoder would eliminate this cost, but has not yet been implemented. Accordingly, the simulation is clearly limited in system size for low error rates.

To obtain results for larger system sizes we replace the ϕ -automaton by explicitly calculating steady-state field values. The appropriate field for a 3D ϕ -automaton is a superposition of fields decaying as $1/r$, where r represents the Manhattan, or 1-norm, distance from the anyon position. The anyon-move rules are identical to the synchronous CA decoder. The iterative field generation via a CA leads to incomplete convergence of the field leading to fields with lightly shorter range. To incorporate this fact we opted for a explicit field decaying as $1/r^{1.05}$. For details on the field profile and convergence properties we refer to Ref. [14].

Figures A.1a–c show numerical results for the explicit field decoder and the 3D ϕ -automaton decoder with synchronous and asynchronous updates. The average survival time $\langle T(L, p) \rangle$ is fitted according to a scaling law

$$\langle T(L, p) \rangle = A + B(p - p_{\text{fit}})L^{1/\nu} + C(p - p_{\text{fit}})^2 L^{2/\nu} + D L^{-1/\mu}, \quad (\text{A1})$$

where the term $D L^{-1/\mu}$ accounts for finite size effects. The asymptotic crossing of the fitted function at p_{fit} represents the indicated threshold. Table A.1 lists all of the determined values.

As expected, the explicit field and the CA decoder show similar behavior and threshold. This motivates to study the explicit field decoder to learn about the large L behavior, since the simulation can be done more efficiently on a traditional computer architecture. Numerics up to system size $L = 80$ can be found in Fig. A.2d. Fitting Eq. (A1) we obtain threshold values p_{th} from 0.03 % to 0.05 % with measurement errors $q = p$. The range is obtained by excluding different amounts of small system size data and varying the used error ranges p . Based on the fitted thresholds p_{fit} we can estimate the relative factor s between the threshold of the explicit field decoder and the CA decoders. Multiplying the actual threshold p_{th} of the explicit field decoder by the factor s give us an estimate for the explicit threshold of a CA decoder. These threshold values can be found in Table A.1.

2. Further Numerical Results

The dimensionality of a ϕ -automaton determines for which number of dimensions the discretized Poisson equation is solved through the iterative algorithm. For constructing a ϕ -automaton decoder with a time independent parameter c , it seems necessary to choose a three dimensional ϕ -automaton. This seems to be based on the phenomenon that an attractive interaction with a field decaying as $1/r^\alpha$ yields a threshold only if $\alpha \geq 1$ [14]. We expect that the same considerations apply for a dynamical decoder that is constructed from identical update rules. Figure A.2a gives the results for a dynamical decoder

TABLE A.1. Numerical results for various decoder configurations. The factor s_p represents the relative shift in the argument of the survival time connecting results with measurement errors $q = p$ and without measurement errors $q = 0$. The error rate p_{fit} represents the threshold value indicated by fitting Eq. (A1). The factor s_{fit} gives the scaling between the $1/r^{1.05}$ decoder with known threshold p'_{th} and the other decoders. In this way the other thresholds are estimated via $p_{\text{th}} = s_{\text{fit}} \cdot p'_{\text{th}}$.

Decoder	Meas. Err.	Factor s_p	p_{fit} (%)	Factor s_{fit}	p_{th} (%)
$1/r^{1.05}$	$q = p$	—	0.18	1.	0.03–0.05
$1/r^{1.05}$	$q = 0$	1.24	0.34	1.82	0.05–0.09
$1/r$	$q = p$	—	0.19	1.01	0.03–0.05
$1/r$	$q = 0$	1.25	0.22	1.17	0.03–0.06
3D Sync.	$q = p$	—	0.16	0.86	0.03–0.04
3D Sync.	$q = 0$	1.30	0.23	1.24	0.04–0.06
3D Async.	$q = p$	—	0.30	1.62	0.05–0.08
3D Async.	$q = 0$	1.48	0.51	2.74	0.08–0.14

that operators with explicitly calculated field values for different choices of the parameter α . We find that the parameter α has a strong impact on the survival time indeed. The increase of survival time is slowly leveling out for $\alpha > 1$. Our main results have focused on the average survival time. However, also the distribution of survival times is of high importance. Figure A.2b shows that small survival times are indeed reliably suppressed. Unfortunately, simulations below threshold for large system sizes are infeasible due to the high survival times. However, the scaling of the survival time above the threshold gives a good indication of the scaling below the threshold. In Fig. A.2c we see exponential suppression of the survival time, which provides a clear indication for exponentially increasing survival time below the threshold. The finite size effects observed up to system size $L \approx 65$ resemble those found in the non-dynamical setting [14]. The source code for the implementation of our numerics is available under <https://userpage.physik.fu-berlin.de/~herold/dynamical-decoders/>.

Appendix B: Conceptual Characteristics of Dynamical Decoders

The concept of dynamical decoders is motivated by the theory of classical robust memories. In this context, cellular automata (CA) are studied that redundantly store the information in their local state space. Appropriately tailored update rules can correct local errors and can be used for active error correction. Such error correcting features appear in two fundamental varieties. First, there exist automata which are called *eroders* or *washout automata*. Considering a binary CA, the repeated action of an eroder leads to all cells having the value of the initial states majority occupation. In this way, eroders are the equivalent of a non-dynamical decoder in the absence of measurement errors. Both systems return a partially erroneous memory state to an error free state. It is suggestive to imagine that in this setting the errors only act at the first time slice and afterwards the eroder can act unimpeded. The second variety appears if we let errors appear at every single time slice. In this setting the following question is asked: Given the initial state is a fixed point of the automaton, is this fixed point stable under local perturbations? This setting corresponds to dynamical decoding where local update rules permanently counteract to the corruption of memory.

Under certain assumptions for dimensional binary CA Toom's theorem applies and being an eroder is equivalent to the existence

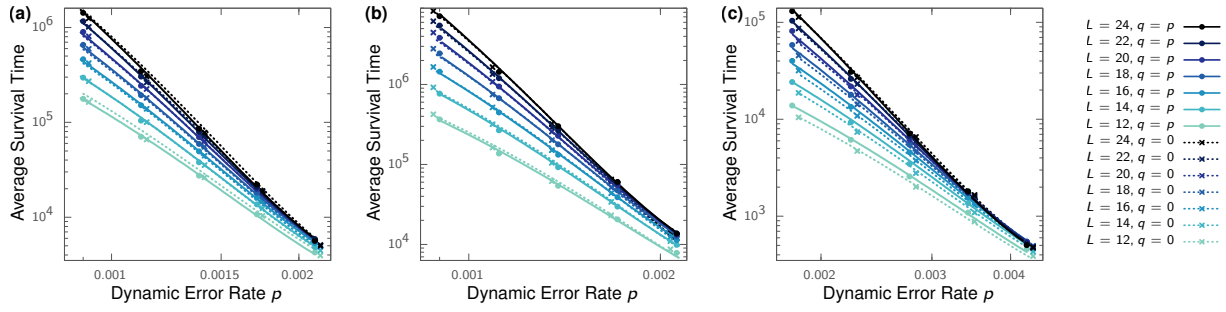


FIG. A.1. Fitted survival times for (a) the $1/r^{1.05}$, (b) the synchronous 3D, and (c) the asynchronous 3D decoder. The data without measurement errors ($q = 0$) are plotted with a shifted error rate $p \rightarrow p/s_p$, such that the two data sets optically match each other.

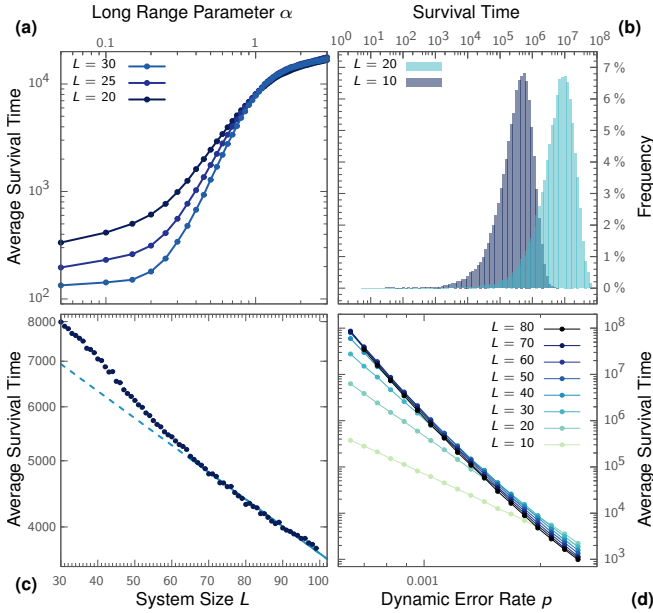


FIG. A.2. Details of dynamical decoders simulated with explicit fields with $1/r^\alpha$ profile and without measurement errors. (a) Survival time for different values of α with $p = 0.6\%$. All other plots with $\alpha = 1.05$, which emulates the 3D ϕ -automaton decoder. (b) Distribution of survival times with $p = q = 0.06\%$. (c) Exponentially decreasing survival time above threshold with $p = q = 0.2\%$. (d) Indication of a threshold between 0.03 and 0.05%.

of stable fixed points. The most prominent example of such a CA is the North-East-Center (NEC) rule, also referred to as Toom's rule. It updates each cell by majority of the three (NEC) cells. For an initial i.i.d. configuration with probability p , the automaton calculates the majority if $p \neq 1/2$, i.e. the automaton is an eroder. This corresponds to a decoder with threshold $p_{th} = 1/2$. Considering the symmetry of the update rule and employing Toom's theorem it follows that the automaton must possess two robust fixed points. However, it is implausible, that the system can tolerate an error rate close to $1/2$ at every time step. This intuition can be made rigorous in the proof of phase coexistence. Consequently, the threshold for the fault tolerance of attractive states has to be lower than $1/2$. This lower threshold would correspond to the threshold of a dynamical decoder.

Using these insights into classical CA, we formulate the following rules of thumb for dynamical decoders: First, a dynamical decoder will usually also work as non-dynamical decoder. And second, the

dynamical threshold is lower than the non-dynamical threshold. To avoid confusion, it should be stated that survival time simulations can also be performed with non-dynamic decoders. Here, both the decoding without measurement errors and the decoding in $2 + 1$ dimensions with measurement errors classify as non-dynamic. For such experiments the decoder threshold and the survival time threshold is identical.

In the main text we consider dynamical decoders in the presence of measurement errors and discuss how measurement errors are equivalent to an increase in physical error rate. Here we substantiate this claim by presenting numerics on dynamical decoders with perfect measurements. When considering perfect measurements, all other aspects are kept the same, including that physical errors can occur at various stages of the decoding process. Our results are shown in Fig. A.1b–c. It is remarkable that over a wide range of parameters (error rates and lattice sizes) the effect of measurement errors is captured by a constant shift in failure probability.

Appendix C: Quantum Dissipative Processes

In this section we discuss in more detail the asynchronous situation that can be interpreted as actual dissipative Markovian dynamics. Consider a continuous-time classical stochastic process in which the unitary O is applied to a quantum system at random times, uniformly distributed at a constant rate $\lambda > 0$, such that the number of events in time interval $(t, t + \tau]$ follows a Poisson distribution with associated parameter $\lambda\tau$. This classical stochastic process is on average on the level of the quantum system reflected by a quantum Markov process: This is a dynamical semi-group, reflected by an equation of motion

$$\frac{\partial \sigma}{\partial t} = \mathcal{L}(\sigma) \quad (C1)$$

where \mathcal{L} is the Liouvillian decomposed for such unitary processes as

$$\mathcal{L}(\sigma) = \gamma \left(O\sigma O^\dagger - \sigma \right). \quad (C2)$$

This can readily be identified as a Liouvillian that takes the form of a Lindblad master equation with rate γ and a single Lindblad operator constituted by the unitary $L = O$. This reasoning can be applied to any unitary applied to any site of the lattice.

Similarly, the purely classical part can be embedded in a quantum system, as has been described in the main text, the involved quantum states being diagonal. In this picture, there is a quantum mechanical equivalent T_x of an update rule f_x at a site x acting as

$$\rho \mapsto T_x \rho T_x^\dagger \quad (C3)$$

on quantum states ρ . Again, if the rule f_x is applied in a continuous asynchronous fashion at rate $\lambda > 0$, this is reflected by the quantum dynamical semi-group of the above form with Lindblad operators $L_x = T_x$. The overall asynchronous cellular automaton can be embedded in a tri-partite quantum system with Hilbert space $\mathcal{H} \otimes \mathcal{L} \otimes \mathcal{V}$, with Lindblad operators $\{L_j\}$ acting locally and at two tensor factors at the time. The actual physical noise process is acting only on the first tensor factor \mathcal{H} associated with the physical quantum degrees of freedom.

Appendix D: Variants of the Asynchronous 3D ϕ -Automaton Decoder

The presented numerics are focused on a certain instance of the asynchronous 3D ϕ -automaton as dynamical decoder. However, we have also considered some variations of the decoder that might simplify the implementation in chips or physical systems. The tested variations cover the following move rules:

- (i) The movement of anyons can be separated in horizontal and vertical moves on the lattice. This yields two distinct operators a_x^h and a_x^v . In this case only two ϕ -values are involved in the determination of the move direction. The feasibility of those rules can be understood by simple heuristics: If, for example, an anyon should not move horizontally at all, it might move horizontally nevertheless. However, this move will be corrected in the next application of either the horizontal or the vertical update.
- (ii) If setting (i) is chosen, the decision in which direction to move, can be made probabilistic based on the field gradient. Since the move rules are split in a_x^h and a_x^v , we obtain a decision that is effectively one dimensional. For this situation we define $\Delta = \phi(x+1) - \phi(x-1)$. In case $\Delta < 0$ the *correct* move direction would be left, and vice versa. The anyon moves in the correct direction with probability

$$\frac{|\Delta| \log^2 L}{|\Delta| \log^2 L + 1}, \quad (D1)$$

and in the *wrong* direction with probability

$$\frac{1}{|\Delta| \log^2 L + 1}. \quad (D2)$$

We believe that the system size dependence of such a probabilistic rule cannot be avoided in our ϕ -automaton decoders.

We also believe that the following adjustments for the field updates will still yield a threshold:

- (i) We expect that it should be possible to reduce the third dimension to a size of $L_3 \sim \log^2 L$, instead of $L_3 = L$. This is motivated by the intuition that only $\log^2 L$ updates are performed to generate the required field. During those updates, informations from cells with a distance larger than $\log^2 L$ cannot influence the central layer. Numerics seem to support this intuition. However, the asymptotic behavior might be revealed only for very large system sizes. There, the field values from previous sequences may influence the fields profile.
- (ii) The local field update involves the value of six neighboring sites and the local charge value. The following rules may reduce the number of involved values from seven to four. To this end we introduce three local cache-variables. These cache-variables are updated with the sum of two neighboring ϕ -values

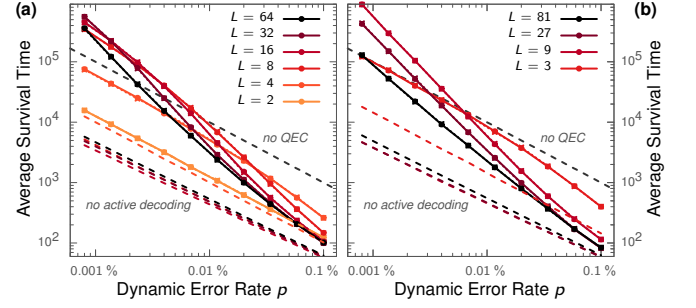


FIG. E.1. Survival time as a function of the error rate for our variant of Harrington's directed signaling decoder with $\text{WORK_PERIOD} = 6$ and colony size 2×2 (a) and 3×3 (b). The results for $q = p$ (filled circle/solid lines) and $q = 0$ (crosses/dashed lines) are almost indistinguishable.

divided by 6. The actual ϕ -value at each site can then be calculated as the sum of those three cache-variables plus the local charge value.

Note that all these adjustments and optimizations can be applied in the non-dynamical setting as well.

Appendix E: Directed Signaling Decoder

Reference [22] provides a numerical benchmark for a dynamical decoder based on directed signaling. The algorithm is partially motivated by the work of Gács [30–32]. The numerical results suggest that the threshold could lie between 0.01 % and 0.1 %. However, the definition of survival in this work is defined via the fidelity of the physical qubits. It is unclear to the authors how this quantity can give a reliable answer to the question if this state can still be decoded correctly.

Here, we give a detailed description of a simplified version of the originally proposed decoder of Ref. [22]. We benchmark this decoder with a colony size of 2×2 and find an indications for a threshold below $p = 0.001$ %. For colony size 3×3 we do not find a threshold in the simulated error range. The presence of measurement errors seems to have almost no impact on the decoder. For details see Fig. E.1. By construction, we expect our variant of this decoder to have a significantly lower threshold. The reason is that we avoid the definition of deviating update rules for the lowest hardware layer to simplify the update rules. This comes at a price: To remove a single bit-flip error, six sequences are required. Therefore, it can be expected that the threshold is lowered by a factor of 1/6. Our implementation possesses further simplifications, especially in the algorithm that determines the anyon presence inside a colony. Before giving the concrete update rules, we explain the underlying concept in abstract terms. Since the construction is only sketched in Ref. [22], we believe that the detailed description laid out below has significant merits in its own right.

1. Basic Concept

The underlying concept of this decoder is the binning of errors into *level- ℓ errors*. We will not make this concept precise but rather use it to motivate the construction of this decoder. Level-0 errors are isolated bit flips resulting in two neighboring anyons. For larger errors

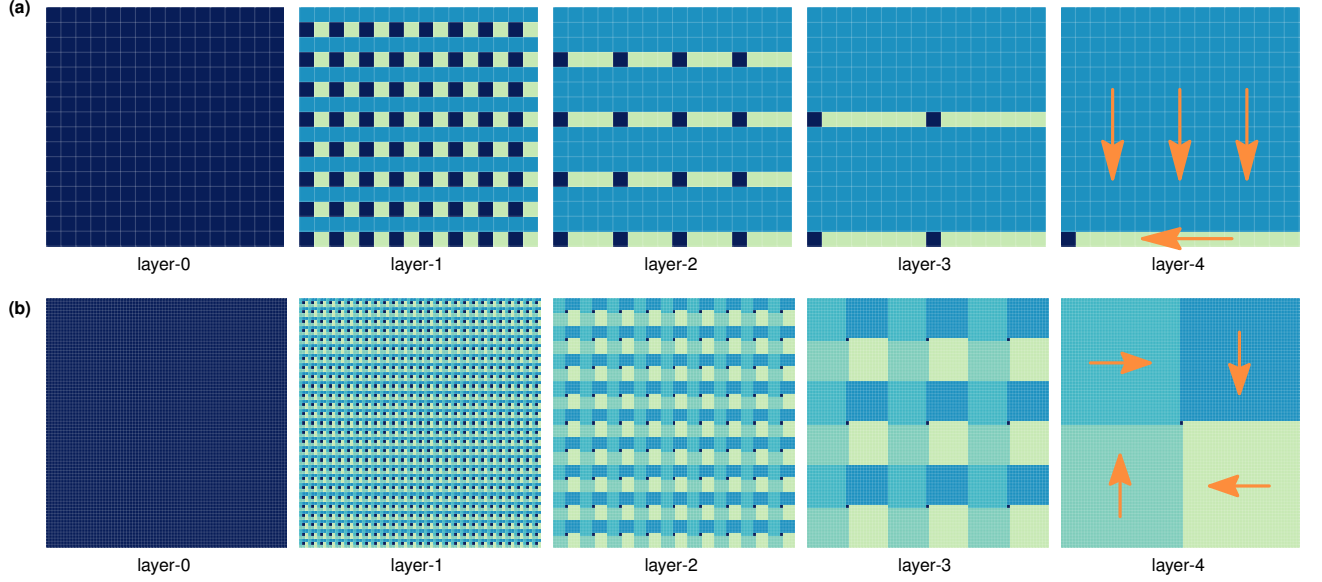


FIG. E.2. Colony structure for all layers for (a) colony size 2×2 and $L = 16$, and (b) colony size 3×3 and $L = 81$. The layer- $(\ell + 1)$ structure is the super colony structure of layer- ℓ . The cells shaded with the darkest color are the center cells, the backup move directions (applying for the subjacent layer) indicated via the lighter colors are depicted within the layer-4 colony structure.

we have to introduce a *colony size* denoted as `COLONY_SIZE`. Given a colony size, we say an error string is level- ℓ if the anyon pair has a distance $\approx \text{COLONY_SIZE}^\ell$. This concept of classification of errors is borrowed from the 1D classical case [31, 32].

To correct errors in all the different error levels, we construct a hierarchical structure from bottom to top. We consider a cellular automaton (CA) with cells at each point on the toric code, where an error syndrome is measured. In this way, each cell is responsible for one anyon. The CA is equipped with the same periodic boundary conditions as the toric code. It is easy to construct local rules to remove level-0 errors, essentially the CA has to output flip instructions – which we call `pauliSignals` – for all spins, separating anyons. We imagine that the toric code is lying below the CA. In this way the CA can receive the syndrome information and pass the flip instructions locally.

To get rid of higher level errors, we first group the CA cells in $\text{COLONY_SIZE} \times \text{COLONY_SIZE}$ squares. We call those squares *super colonies*, the naming convention will become clearer soon. For simplicity, we assume that the system size is a power of the colony size, such that $L = \text{COLONY_SIZE}^\Delta$. We give the update rule at each cell a *backup move direction*. This move direction is chosen if the neighborhood of an anyon does not contain another anyon, and it depends on the position of the cell inside the super colony. The backup move directions inside a super colony obey the scheme

$$\begin{array}{|c|c|} \hline \downarrow & \downarrow \\ \hline C & \leftarrow \\ \hline \end{array} \quad \text{and} \quad \begin{array}{|c|c|c|} \hline \rightarrow & \downarrow & \downarrow \\ \hline \rightarrow & C & \leftarrow \\ \hline \uparrow & \uparrow & \leftarrow \\ \hline \end{array} \quad (\text{E1})$$

for colony sizes of two and three. In this way we achieve that all anyons without a direct partner are moved to a certain cell inside the square. The schemes for larger colonies can be constructed accordingly. We refer to the cell C as *super colony center*. Eventually the super colony will contain no anyon or one anyon at the super colony center.

To pair the remaining anyons at the super colony centers we add a CA with the same cell structure on top of the first one. We refer to this

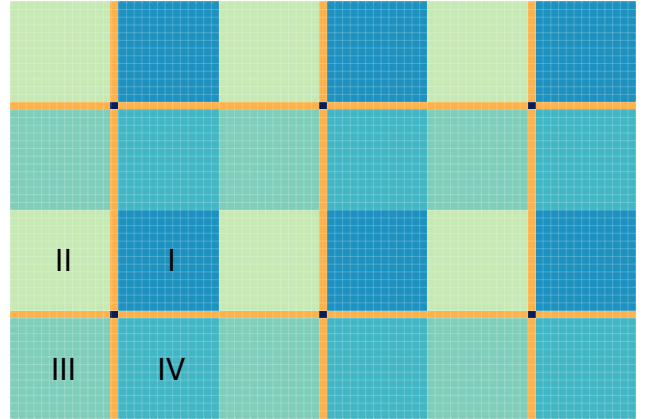


FIG. E.3. Fundamental structure of a layer of the decoder. Dark shaded isolated cells are colony centers. The colored squares represent quadrants of the colony. The colony centers are connected via the yellow marked corridor cells. Note that the corridor cells also belong to one of the quadrants respectively (see Fig. E.2).

CA as *layer-1*. In this layer we directly start by arranging the cells into squares. Particularly, we take the super colony structure from the underlying *layer-0*. But inside of *layer-1* we refer to the super colonies of *layer-0* simply as *colonies*. The singular point of a colony to which all the anyons have moved via *layer-0* is called *colony center* in the context of the *layer-1* CA. Next, we describe how in *layer-1* the correction of level-1 errors is orchestrated. To fuse anyons between neighboring colony centers, the colony center cells perform update rules quite different from those of the other cells. If an anyon is present at a colony center, the information “anyons present” is sent to the neighboring colony centers in each time step. To keep this signaling local, the signals are passed via the intermediate cells using local

TABLE E.1. Local state space and description of the role of the different fields. The size of fields marked with * is layer dependent.

Field	Subfields	Description
counterSignal	toNorth toEast toSouth	Signal to inform neighboring colonies about anyon presence. Transported along corridors and emitted by centers by setting the value. Possible value are 0 (no anyon present) and 1 (anyon present).
flipSignal	toWest toNorth toEast toSouth	Signal that induces a chain of flips along the corridor the signal travels. Flip instructions are stored in the pauliSignal field. Colliding flip signals annihilate each other. Possible values are 0 (no flip) and 1 (flip).
pauliSignal	toWest west south	Stores Pauli operators to apply to the corresponding qubit. The two stored values correspond to the elementary cell of the toric code. Pauli signals travel from top to bottom and are passed to the physical layer eventually. The value 0 corresponds to identity, the value 1 to a Pauli X -operator.
age*	—	Incremented each round and set to 0 if the value $\text{WORK_PERIOD}^{\ell+1}$ is reached. On $\text{age} = 0$ decisions to send flipSignals are made.
syndrome	—	Measured syndrome, passed from the physical layer to the top. Values are 0 (syndrome +1) and 1 (syndrome -1).
counterColony*	—	Incremented if the syndrome is 1.
counterNeighbor*	fromNorth fromEast fromSouth fromWest	Incremented on incoming counterSignals from the corresponding direction.
quadrant	—	Fixed value that contains the cells position inside its super colony. The possible values I, II, III and IV correspond to the corresponding quadrants. The value C is associated to super colony centers.

update rules. We refer to those cells as the *corridor* that connects two centers. In this way, the signals are passed to neighbors along the corridors in COLONY_SIZE time steps. The transmitted information will allow colony centers to detect potential pairing candidates.

Clearly, decisions can not be based on a single “anyons present” signal: We only know that unpaired anyons will reside at the colony center “most of the time”. Also, signals need time to travel from one colony center to the other. Instead of interpreting a single signal, we store the incoming information over a time period at each colony center and eventually infer the actual situation from this history. Practically, each colony center is equipped with five counters. The *colony counter* is incremented each time the underlying layer reports the presence of an anyon. The *neighbor counter* is incremented on incoming “anyon present” signals, where a different counter is maintained for each cardinal direction. The counter values are evaluated after the so called *work period*. In case the counters exceed a certain fraction of the work period, this is interpreted as the presence of an anyon. If the anyon counter and at least one signal counter exceed the threshold, the anyon is moved towards one of the neighboring colonies. If only the anyon counter exceeds the threshold, the anyon is moved towards the center of the super colony (backup move direction) with size $\text{COLONY_SIZE}^2 \times \text{COLONY_SIZE}^2$ (cf. layer-0 rules). The moving of anyons is implemented via *flip signals*, which are not only transported from one colony to the other via a corridor, but also trigger the creation of flip instructions (pauliSignals), which are sent to the bottom layer. Also, colliding flip signals annihilate each other which ensures that two flip signals from neighboring colonies do not reverse the intended effect. Independent of the decision the center cell has computed, all the counters are reset to zero after the work period has ended and thus the counting process is restarted.

To account for arbitrary *level- ℓ* errors up to $\ell = \mathcal{L}$, we add corre-

sponding *layer- ℓ* cellular automata. The colony size for those layers is given by COLONY_SIZE^ℓ , the super colony sizes by $\text{COLONY_SIZE}^{\ell+1}$, and the work period by $\text{WORK_PERIOD}^{\ell+1}$, where the constant WORK_PERIOD depends on the chosen COLONY_SIZE . An illustration of the colony structure can be found in Fig. E.2. Note, that the size of the counter fields in each layer has to increase to store the maximal value of $\text{WORK_PERIOD}^{\ell+1}$. Having defined the update rules in each layer, we can shortly revisit the layer-0 rules. If we apply the previous prescriptions to this layer we obtain a colony of size 1×1 , i. e. a colony which only consists of a single center cell. Within in WORK_PERIOD time steps the centers approximate one time step within the layer-0 rules as defined before.

2. Update Rules

In this section we give an exact definition of a decoder using directed signaling. It is defined for all colony sizes $\text{COLONY_SIZE} \geq 2$ and for system sizes $L = \text{COLONY_SIZE}^{\mathcal{L}}$ with $\mathcal{L} \in \mathbb{N}$. We will note the updates for the different fields of the cells independently and denote them by

$$\text{fieldName} \mapsto \text{new value}. \quad (\text{E2})$$

An overview over all existing fields can be found in Table E.1. The new value can depend on the current state of the field and the state of the six neighboring cells, which are addressed by *north*(·), *east*(·), *south*(·), *west*(·), *above*(·), and *below*(·). Note that the updates are synchronous, which implies that the *new value* expression is only addressing values that have been generated via the previous update. For updates of binary fields we denote the exclusive or between two values – i.e. addition modulo two – by $\cdot \oplus \cdot$.

a. Corridor Rules

The update rule for the `pauliSignal` fields incorporates incoming `flipSignals` into the local Pauli frame. To transport the Pauli operators to the physical layer, the state of the layer above is also incorporated. The rule reads

$$\text{pauliSignal.west} \mapsto \text{above}(\text{pauliSignal.west}) \oplus \text{west}(\text{flipSignal.toEast}), \quad (\text{E3a})$$

$$\text{pauliSignal.south} \mapsto \text{above}(\text{pauliSignal.south}) \oplus \text{south}(\text{flipSignal.toNorth}). \quad (\text{E3b})$$

Corridor cells have the task to transport signals between center cells. The transport of `counterSignal` is implemented via

$$\text{counterSignal.toNorth} \mapsto \text{south}(\text{counterSignal.toNorth}), \quad (\text{E4a})$$

$$\text{counterSignal.toEast} \mapsto \text{west}(\text{counterSignal.toEast}), \quad (\text{E4b})$$

$$\text{counterSignal.toSouth} \mapsto \text{north}(\text{counterSignal.toSouth}), \quad (\text{E4c})$$

$$\text{counterSignal.toWest} \mapsto \text{east}(\text{counterSignal.toWest}). \quad (\text{E4d})$$

For the transport of `flipSignals`, we need to ensure that colliding signals annihilate each other. It is sufficient to cover the case of only two signals that are approaching each other, since only a single signal may be emitted by a center cell per work period. There are two possible cases to be considered. First, the approach that leads to two neighboring cells containing a flip signal, and second the case that leads to one cell containing two flip signals. Considering the update rules

$$\text{flipSignal.toNorth} \mapsto \begin{cases} \text{south}(\text{flipSignal.toNorth}) & \text{north}(\text{flipSignal.toSouth}) = 0 \wedge \text{flipSignal.toSouth} = 0 \\ 0 & \text{otherwise,} \end{cases} \quad (\text{E5a})$$

$$\text{flipSignal.toEast} \mapsto \begin{cases} \text{west}(\text{flipSignal.toEast}) & \text{east}(\text{flipSignal.toWest}) = 0 \wedge \text{flipSignal.toWest} = 0 \\ 0 & \text{otherwise,} \end{cases} \quad (\text{E5b})$$

$$\text{flipSignal.toSouth} \mapsto \begin{cases} \text{north}(\text{flipSignal.toSouth}) & \text{south}(\text{flipSignal.toNorth}) = 0 \wedge \text{flipSignal.toNorth} = 0 \\ 0 & \text{otherwise,} \end{cases} \quad (\text{E5c})$$

$$\text{flipSignal.toWest} \mapsto \begin{cases} \text{east}(\text{flipSignal.toWest}) & \text{west}(\text{flipSignal.toEast}) = 0 \wedge \text{flipSignal.toEast} = 0 \\ 0 & \text{otherwise.} \end{cases} \quad (\text{E5d})$$

it is easy to verify that colliding signals are annihilated.

b. Center Rules

At center cells the outcome of the syndrome measurement at the corresponding check operator has to be known. This information is transported upwards via

$$\text{syndrome} \mapsto \text{below}(\text{syndrome}), \quad (\text{E6})$$

originating from the physical layer. To perform certain operations every $\text{WORK_PERIOD}^{\ell+1}$ steps, we keep track of the time inside each center via

$$\text{age} \mapsto \text{age} + 1 \mod \text{WORK_PERIOD}^{\ell+1}. \quad (\text{E7})$$

To determine if action is required the presence of anyons inside the colony has to be detected. Therefore, the number of `syndrome = 1` events is tracked via the `counterColony` field with the update rule

$$\text{counterColony} \mapsto \begin{cases} 0 & \text{age} = 0 \\ \text{counterColony} + \text{below}(\text{syndrome}) & \text{otherwise.} \end{cases} \quad (\text{E8})$$

To determine potential neighboring anyons to pair with, the `counterSignals` from neighboring colonies are tracked via

$$\text{counterNeighbor.fromNorth} \mapsto \begin{cases} 0 & \text{age} = 0 \\ \text{counterNeighbor.fromNorth} + \text{north}(\text{counterSignal.toSouth}) & \text{otherwise,} \end{cases} \quad (\text{E9a})$$

$$\text{counterNeighbor.fromEast} \mapsto \begin{cases} 0 & \text{age} = 0 \\ \text{counterNeighbor.fromEast} + \text{east}(\text{counterSignal.toWest}) & \text{otherwise,} \end{cases} \quad (\text{E9b})$$

$$\text{counterNeighbor.fromSouth} \mapsto \begin{cases} 0 & \text{age} = 0 \\ \text{counterNeighbor.fromSouth} + \text{south}(\text{counterSignal.toNorth}) & \text{otherwise,} \end{cases} \quad (\text{E9c})$$

$$\text{counterNeighbor.fromWest} \mapsto \begin{cases} 0 & \text{age} = 0 \\ \text{counterNeighbor.fromWest} + \text{west}(\text{counterSignal.toEast}) & \text{otherwise.} \end{cases} \quad (\text{E9d})$$

With the beginning of each work period ($\text{age} = 0$), the counters are reset.

The flip signals sent by center cells contain the current state of the incoming syndrome field. To actually *send* a signal, it is sufficient to just set the `counterSignal` values at the center to the desired value. The neighboring corridor cells will pick up this signal subsequently. Hence, the update rules must read

$$\text{counterSignal.toNorth} \mapsto \text{below}(\text{syndrome}), \quad (\text{E10a})$$

$$\text{counterSignal.toEast} \mapsto \text{below}(\text{syndrome}), \quad (\text{E10b})$$

$$\text{counterSignal.toSouth} \mapsto \text{below}(\text{syndrome}), \quad (\text{E10c})$$

$$\text{counterSignal.toWest} \mapsto \text{below}(\text{syndrome}). \quad (\text{E10d})$$

Finally, we have to define in which cases `flipSignals` are emitted from the center cells. For this purpose we first define the counter threshold $\text{th} := \frac{3}{4} \cdot \text{WORK_PERIOD}^{\ell+1}$. The following quantity gives detailed information about the chosen direction for flip signals:

$$\text{direction} := \begin{cases} \text{NONE} & \text{age} \neq 0 \vee \text{counterColony} < \text{th} \\ \text{NORTH} & \text{counterNeighbor.north} \geq \text{th} \\ \text{EAST} & \text{counterNeighbor.east} \geq \text{th} \\ \text{SOUTH} & \text{counterNeighbor.south} \geq \text{th} \\ \text{WEST} & \text{counterNeighbor.west} \geq \text{th} \\ \text{BACKUP_NORTH} & \text{quadrant} = \text{III} \\ \text{BACKUP_EAST} & \text{quadrant} = \text{II} \\ \text{BACKUP_SOUTH} & \text{quadrant} = \text{I} \\ \text{BACKUP_WEST} & \text{quadrant} = \text{IV}. \end{cases} \quad (\text{E11})$$

The first condition “ $\text{age} \neq 0 \vee \text{counterColony} < \text{th}$ ” ensures that flip signals are only emitted at the beginning of work periods and only if an anyon was present in the colony for most of the time. There are two cases in which flip signals are emitted. The first case occurs if the neighbor counter for the corresponding direction exceeds the threshold. If multiple neighbor counters exceed the threshold, signals to the direction north, east, south, and west are preferred according to this order. The second case occurs if all neighbor counters are below the threshold. In this case a flip signal is emitted to move the anyon closer towards the super colony center. This decision is based on the quadrant value. See Figs. E.2–E.3 for a graphical description of quadrants and backup move directions.

The following rules are responsible for sending out the corresponding flip signals:

$$\text{flipSignal.toNorth} \mapsto \begin{cases} 1 & \text{direction} = \text{NORTH} \vee \text{direction} = \text{BACKUP_NORTH} \\ 0 & \text{otherwise,} \end{cases} \quad (\text{E12a})$$

$$\text{flipSignal.toEast} \mapsto \begin{cases} 1 & \text{direction} = \text{EAST} \vee \text{direction} = \text{BACKUP_EAST} \\ 0 & \text{otherwise,} \end{cases} \quad (\text{E12b})$$

$$\text{flipSignal.toSouth} \mapsto \begin{cases} 1 & \text{direction} = \text{SOUTH} \vee \text{direction} = \text{BACKUP_SOUTH} \\ 0 & \text{otherwise,} \end{cases} \quad (\text{E12c})$$

$$\text{flipSignal.toWest} \mapsto \begin{cases} 1 & \text{direction} = \text{WEST} \vee \text{direction} = \text{BACKUP_WEST} \\ 0 & \text{otherwise.} \end{cases} \quad (\text{E12d})$$

It is crucial to incorporate the emitted flip signals into the local Pauli frame in a certain way. Therefore, the `pauliSignal` update rules read

$$\text{pauliSignal.west} \mapsto \text{above}(\text{pauliSignal.west}) \oplus \text{west}(\text{flipSignal.toEast}) \quad (\text{E13a})$$

$$\oplus \begin{cases} 1 & \text{direction} = \text{BACKUP_WEST} \\ 0 & \text{otherwise,} \end{cases}$$

$$\text{pauliSignal.south} \mapsto \text{above}(\text{pauliSignal.south}) \oplus \text{south}(\text{flipSignal.toNorth}) \quad (\text{E13b})$$

$$\oplus \begin{cases} 1 & \text{direction} = \text{BACKUP_SOUTH} \\ 0 & \text{otherwise.} \end{cases}$$

These specific rules are required to make the rules work as layer-0 rules too. If two neighboring anyons try to fuse the conditional terms in Eqs. (E13a)–(E13b) are irrelevant. Clearly, only one cell will incorporate the signal into the local Pauli frame, which is the desired behavior for level-0 corrections. If backup move directions are used, no neighboring cell issues the reverse signal. Thus, if the signal must effect the local Pauli frame (only west and south signals), this has to be implemented explicitly as it has been done via the conditional part of the update rule.